EFFECT OF PREPARATION METHOD IN THE PROPERTIES OF IRON OXIDE CATALYSTS FOR FENTON REACTION

EFEITO DO MÉTODO DE PREPARAÇÃO NAS PROPRIEDADES DOS CATALISADORES DE ÓXIDO DE FERRO PARA A REAÇÃO DE FENTON

F. M. BARBOSA and A. R. MARTINS[*]

Instituto Federal da Bahia – Campus Porto Seguro, s/n, Fontana 1, Cep. 45810-000, Porto Seguro, BA – Brazil.

[*] Corresponding author: Instituto Federal da Bahia – Campus Porto Seguro, s/n, Fontana 1, Cep. 45810-000, Porto Seguro, BA – Brasil, Phone: +55 73 988344197
e-mail addressl: andremartins@ifba.edu.br (A. R. Martins).

ABSTRACT

This work discusses methods of preparing iron oxide for the Fenton reaction, using methylene blue as a model molecule. The solids were prepared by precipitation, complexation, combustion, and decomposition and characterized by Fourier transform infrared spectroscopy, X-ray diffraction, scanning electronic microscopy, energy dispersive X-ray spectroscopy, specific surface area measurement and were evaluated for methylene blue removal. The method influenced the structural and surface properties of the solids, and consequently the catalytic performance of the solids. The solid prepared by precipitation showed the highest area, amorphous phase, and the best performance in the adsorption test. On the other hand, the combustion method favored the formation of hematite and traces of magnetite. The solid prepared by this method showed higher values of the methylene blue dye oxidation.

.

RESUMO

Este trabalho discute métodos de preparação de óxido de ferro para a reação de Fenton, utilizando o azul de metileno como molécula modelo. Os sólidos foram preparados por precipitação, complexação, combustão e decomposição e caracterizados por espectroscopia de infravermelho por transformada de Fourier, difração de raios-X, microscopia eletrônica de varredura, espectroscopia de energia dispersiva de raios-X, medição de área superficial específica e foram avaliados para remoção de azul de metileno. O método influenciou as propriedades estruturais e superficiais dos sólidos e, consequentemente, o desempenho catalítico dos sólidos. O sólido preparado por precipitação apresentou a maior área, fase amorfa e melhor desempenho no teste de adsorção. Por outro lado, o método de combustão favoreceu a formação de hematita e vestígios de magnetita. O sólido preparado por este método apresentou valores mais altos de oxidação do azul de metileno.

.

1. INTRODUCTION

Due to the growing need for procedures which show higher efficiency in wastewater treatment, several techniques have been tested in recent decades (MANENTI et al., 2010; PALÁCIO et al., 2015). The most effective processes, called Advanced Oxidative Processes (AOPs), have become alternatives for treating recalcitrant, hydrophobic and bioaccumulative organic compounds which have high chemical and photochemical stability, together with very slow biodegradation rate (NOGUEIRA et al., 2007; SILVA et al., 2002). The AOPs constitute a promising technology that formation of hydroxyl radicals, oxidizing chemical species, capable of degrading highly stable organic contaminants. In addition, Advanced Oxidation Processes can be used in conjunction with biological treatments to increase the biodegradability of recalcitrant compounds, thereby reducing the required treatment time via traditional biological processes (DENG; ZHAO, 2015; NOGUEIRA et al., 2007).

The Fenton homogeneous system is widely used to degrade various contaminants in industrial effluents. This reaction occurs in the presence of ferrous (Fe^{2+}) or ferric (Fe^{+3}) ions with hydrogen peroxide (H_2O_2).The classic mechanism is a simple redox reaction in which Fe^{2+} ions are oxidized to Fe^{+3} ions and hydrogen peroxide is reduced to hydroxyl ion (-OH) and a hydroxyl radical (•OH) (equations 1 to 2). Although highly efficient, this system has some drawbacks, such as the need of pH close to 3 for iron ions to be soluble, residue formation at neutralization step and catalyst recovery difficulty (DENG; ZHAO, 2015; DURIGAN; VAZ; PERALTA-ZAMORA, 2012; MACHULEK et al., 2013).

$$Fe^{2+} + H_2O_2 \rightarrow Fe^{3+} + \text{-OH} + \text{•OH} \qquad (1)$$

$$Fe^{3+} + H_2O_2 \rightarrow FeOOH^{2+} + H+ \qquad (2)$$
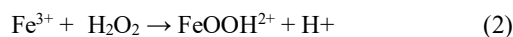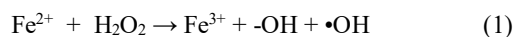
Due to these disadvantages, the heterogeneous Fenton system has emerged as an alternative to homogeneous Fenton process. Reactions involving the formation of hydroxyl radical catalyzed by solid iron compounds such as goethite, hematite, magnetite and iron hydroxides, supported by activated carbon, silica, alumina, among others, have received special attention from researchers. This is due to the advantages over the classic homogeneous process involving soluble iron salts, since the pH

control step around 3 and subsequent neutralization can be avoided, reducing waste generation and promoting catalyst recovery at the end of the process (DURIGAN; VAZ; PERALTA-ZAMORA, 2012; NOGUEIRA et al., 2007; OLIVEIRA; FABRIS; PEREIRA, 2013). Chemical species based on iron are more active in the Fenton and photo-Fenton reaction. In addition, the use of iron oxides has low cost, low toxicity and it is easy to recover (HE et al., 2016).

In this sense, studies involving iron oxide catalysts preparation methods are especially convenient when the purpose is to produce solids with promising catalytic properties (GONÇALVES et al., 2009; ZANINI et al., 2017). The choice of preparation method may have a significant effect on catalyst activity and selectivity because of the different particle sizes and phases formed in the solids, among other characteristics that vary with the preparation method. In addition, multi-step methods can lead to increased cost and waste (GONÇALVES et al., 2009; SANTOS; SILVA, 2015). Therefore, it is convenient to search for simple methods which result in low residue formation, low cost and which are efficient for catalysts with optimized properties.

Some methods of preparing catalysts have stood out because they have easy reproduction, low cost, and low waste production. Among them, combustion, complexation, decomposition and precipitation (PEREIRA et al., 2008). The method of precipitation with ammonia and pH control facilitates the control of particle size, and favors an increase in the area of solids (ADANS et al., 2016; CARVALHO et al., 2009; SILVA et al., 2017). A little more laborious, the method using citric acid is still not well explored, requiring further investigation (LIU et al., 2020). The use of citric acid to form complexes that precede the formation of catalysts based on transition metals results in a more homogeneous chemical environment (ASSAF et al., 2008). Finally, the combustion method can favor the formation of nanoparticles (WANG et al., 2017). In addition, it stands out for being carried out in a very short time.

Thus, the aim of this work is the scientific and technological knowledge generation regarding iron oxide based catalysts produced by different methods and to evaluate them in Fenton reaction.

2. MATERIAL AND METHODS

1.1 Catalyst Preparation

The solids were prepared by different methods: precipitation, complexation, combustion, and decomposition.

To produce iron oxides by precipitation method, 100 mL 1.0 molL^{-1} iron (III) nitrate nonahydrate solution and ammonium hydroxide solution (38% v / v) were added to a beaker containing 50 mL water under constant stirring at room temperature. The pH was kept at 11 until complete addition of the reactants. The precipitate formed was stirred for 15 min, then

vacuum filtered, and oven dried at 120 °C for 24 h. Finally, the solid was calcined, generating the Fe-PHA sample.

In order to produce iron oxides by complexation method, 100 mL 1.0 mol L^{-1} iron nitrate nonahydrate solution and 100 mL 3.0 molL^{-1} citric acid solution were added to a beaker, with 3:1 citric acid/metal molar ratio for citratometallic production under constant stirring at room temperature. Subsequently, 0.6 mol ethylene glycol solution under constant stirring was added to citrate complex solution to promote polymerization by

ethylene glycol citric acid reaction. The obtained material was heated to 90 °C under stirring to remove excess water. The remaining moisture was removed in an oven at 120 °C for 24 h from which a resin was produced. This polymerized matrix was then calcined generating the Fe-CX sample.

The iron oxides preparation by combustion method occurred by dissolving 0.1 mol iron nitrate nonahydrate in 20 mL distilled water under constant stirring. Then, 0.375 mol urea was added to follow the oxidant to fuel stoichiometric ratio. The mixture was heated to 90 °C in small quantities in porcelain crucibles to remove excess water. Subsequently, the mixture was taken to the muffle furnace at 300 °C to combustion. The combustion product was calcined generating the Fe-CB sample.

In order to produce iron oxides by decomposition method, 0.1 mol iron nonahydrate nitrate was added to a mortar. Then, with the aid of a pistil, the salt was macerated to ensure its homogeneity. The resulting mixture was calcined generating the Fe-DN sample.

All samples were calcined at 400 °C for 2h at heating rate 2 °C min^{-1}.

1.1 Catalysts characterization

In addition to yield calculations, solids were characterized by X-ray diffraction (XRD), Fourier transform infrared spectroscopy (FT-IR), scanning electronic microscopy (SEM), X-ray energy dispersion spectroscopy (EDS), specific surface area measurement (Sg) and catalytic activity evaluation for Fenton reaction.

The yield calculations were obtained by the ratio between the experimentally obtained mass after the calcination step and the expected mass, considering the Fe_2O_3 iron oxide production. For example, according to the reaction stoichiometry, 404 grams of Fe $(NO_3)_3.9 H_2O$ produces 70 grams of Fe_2O_3. Thus, the yield presented the percentage of mass obtained in relation to the expected mass.

The samples XRD measurements were performed using a XRD600 Shimadzu diffractometer with nickel filter. The sample was exposed to CuKα radiation (λ = 1.5406) generated at 30 kV and 20 mA. The scan was performed at 2θ range from 10° to 80°. The samples structural characterization was performed through crystalline phase identification with automatic search using a Match3 Inorganic Crystal Structure Database (ICSD). In addition, through XRD analyzes it was possible to estimate the crystals average size of solids obtained by Scherrer equation.

Spectra were generated in the mid-infrared region, at the range 4000 to 400 cm^{-1} by means of Spectrum100-FT-IR Fourier-PERKIN ELMER analyzer. The solids were analyzed as pellets from the diluted potassium bromide sample at 200:1 ratio, using 4 cm^{-1} resolution and 32 scans accumulation. The equipment operated in an environment at around 22 ºC and relative air humidity below 50%.

Scanning electron microscopy (SEM) images were obtained using 15 kV VEJA 3 Tesca equipment and X-ray dispersive spectroscopy analyzes were performed in a X-act Oxford Instruments apparatus coupled to the scanning electronic microscope.

The catalysts textural properties were determined by nitrogen cracking experiments carried out at 196 °C in a Micromeritcs ASAP 2020. The specific surface area was calculated by the Brunauer-Emmett - Teller (BET) model and the distribution pore size and volume were calculated using the Barret - Joyner - Halenda (BJH) method.

1.1 Catalytic activity measure

Spectrophotometric measurements were performed following Lambert-Beer law in a IL-226-BI UV-VisKasuaki spectrophotometer, with 0.5 cm optical path glass cuvettes, at different predetermined time intervals and pH was verified by a HI 8224 HANNA pH meter.

Reactions were performed using 15 mL from 10 mgL^{-1} methylene blue dye solution and 1 mL 30% hydrogen peroxide solution under stirring at pH 6 ± 0.4 at 27 ± 1 ºC and relative humidity of 84%. Aliquots were taken at pre-established time intervals. Spectrophotometric measurements were performed at 666 nm wavelength.

To evaluate the solids as adsorbents, 0.03 g of each sample was previously saturated with 15mL from 10 mg L^{-1} methylene blue dye solution and aliquots were taken at the predetermined intervals. The adsorption tests were done in batches, varying the contact time from 15 to 180 min (3 h) with additional 10 min in the centrifuge after each time interval at 1300 rpm. Methylene blue concentration was measured using a UV-Vis spectrophotometer at 666 nm wavelength. The amount of dye adsorbed by the solid, qe (mg g^{-1}), was calculated based on the equation proposed in the literature (GONÇALVES et al., 2009).

Oxidation analyzes were conducted under the same conditions by adding 100 µL hydrogen peroxide (30%, v / v). The samples pH when necessary were adjusted with 0.1 $molL^{-1}$ sulfuric acid and / or 0.1 $molL^{-1}$ sodium hydroxide solutions. Removal percentage was determined based on absorbance conversion values as a concentration percentage at each time interval.

3. RESULTS AND DISCUSSION

Table 1 presents the yield values obtained from solid synthesis, calculated based on the amount of product after the calcination step and the expected value based on the proposed reactions stoichiometry. Most methods led to high yield values above 80%.

FTIR spectra (Figure 1) showed weak absorption bands of 3456-3440 cm^{-1} attributed to the -OH group stretch vibration mode present on the oxide surface. The absorption bands at approximately 1635-1630 cm^{-1} are attributed to the -OH group deformation vibration mode from water molecules adsorbed on the metal oxides hydrophilic surface (ZIMMERMANN et al., 2019). The band at 1385 cm^{-1} corresponds to nitrate groups stretching vibration in inorganic complexes, with different coordination modes on the iron oxide surface. This may indicate that the calcination temperature was not enough to eliminate all nitrate ions from the precursor salts (PEREIRA et al., 2008).

The absorption bands from 600 to 550 cm^{-1} are commonly attributed to the Fe-O group stretch vibration mode characteristic of the magnetite phase, corresponding to the bonds vibration between Fe^{2+} and O^{2-} ions, in which the metal occupied octahedral sites. The absorption bands corresponding to the bonds vibration between Fe^{3+} and O^{2-} are located at approximately 450-335 cm^{-1} (GARCÍA CERDA, 2005; PEREIRA et al., 2008).
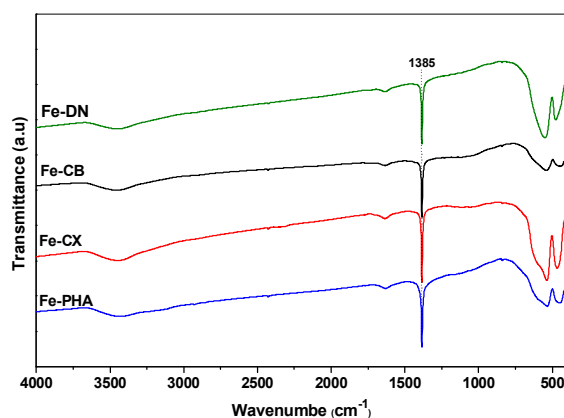
Figure 1 - FTIR spectra of catalysts produced by complexation (Fe-CX), iron nitrate decomposition (Fe-DN), precipitation (Fe-PHA) and combustion (Fe-CB).

X-ray diffractograms (Figure 2) indicate that in solids obtained by complexation, combustion and decomposition methods, the formation of the major hematite phase (α-Fe$_2$O$_3$) with trigonal structure (rhombohedral axes) and magnetite (Fe$_3$O$_4$) or maghemite (γ-Fe$_2$O$_3$) at $2\theta = 35.54°$ and $62.36°$ occurred. Magnetite (Fe$_3$O$_4$) and maghemite (γ-Fe$_2$O$_3$) have similar spinel-like crystallographic structures, so it is not possible to differentiate them by diffractogram (OLIVEIRA; FABRIS; PEREIRA, 2013). However, according to other authors (SCHWERTMANN, 2000), maghemite (γ-Fe$_2$O$_3$) is a dark brown solid while magnetite (Fe$_3$O$_4$) is black (FERREIRA et al., 2007). Figure 3 shows the color of samples obtained by different methods. From the staining of the samples obtained, the species present in samples Fe-CX and Fe-DN is possibly maghemite while in sample Fe-CB it is magnetite. These same results were also confirmed by other authors (Schwertmann and Cornell, (2000)). However, regarding Fe-PHA sample, XRD profiles indicated the formation of amorphous halo. Thus, from the results of X-ray diffraction diffraction, it can be concluded that the preparation of solids by different methods favored hematite (α-Fe$_2$O$_3$) formation, with traces of magnetite (Fe$_3$O$_4$) and of maghemite (γ-Fe$_2$O$_3$) for Fe-CB, Fe-CX and Fe-DN samples.

Table 1 – Yield and textural properties of solids: TC (average size of crystals), Sg (specific surface area), VP (pore volume) and TP (average pore size).

Samples	Yield (%)	TC (nm)	Sg (m^{2}g^{-1})	VP (cm^3.g^{-1})	TP (nm)
Fe-PHA	87	n.d.	24	0.142	17
Fe-CX	83	29	16	0.0780	30
Fe-DN	95	29	15	0.0774	22
Fe-CB	90	29	3	0.0082	12

* n.d.= not determined.

After phase identification, the crystals average size present in the iron oxide powders obtained by complexation (Fe-CX), combustion (Fe-CB) and decomposition (Fe-DN) methods was performed using Scherrer equation (HEITMANN et al., 2014). For the sample obtained by precipitation method (Fe-PHA), the calculation was not possible because XRD analysis indicated an amorphous halo profile. Furthermore, the results indicated that all powders, composed by nanocrystals, did not show significant average crystal sizes variations (MAGALHÃES et al., 2007).

The specific surface area values were performed by the BET method and are shown in Table 1. It can be observed that the area varied according to the method. Fe-PHA sample showed a higher area (24 m^{2}g^{-1}) which may be related to structure disorganization, as shown by XRD results. It is also observed that the Fe-CB sample had lower specific surface area values (3 m^{2}g^{-1}) than the others. This fact is justified by the release of energy in the combustion stage which favors the material sintering thus reducing the specific area (SILVA et al., 2017). However, complexing and decomposition methods from iron nitrate resulted in solids with close area values. Consistent with the area values, the Fe-PHA sample showed an average pore volume significantly higher than the others. On the other hand, the Fe-CB sample showed lower volume and pore size values. Therefore, although the combustion method may favor the formation of magnetite (phase desirable for Fenton) (PĂCURARIU et al., 2016) as shown by the XRD results, it is common to undermine the textural properties of the catalysts due to sintering.
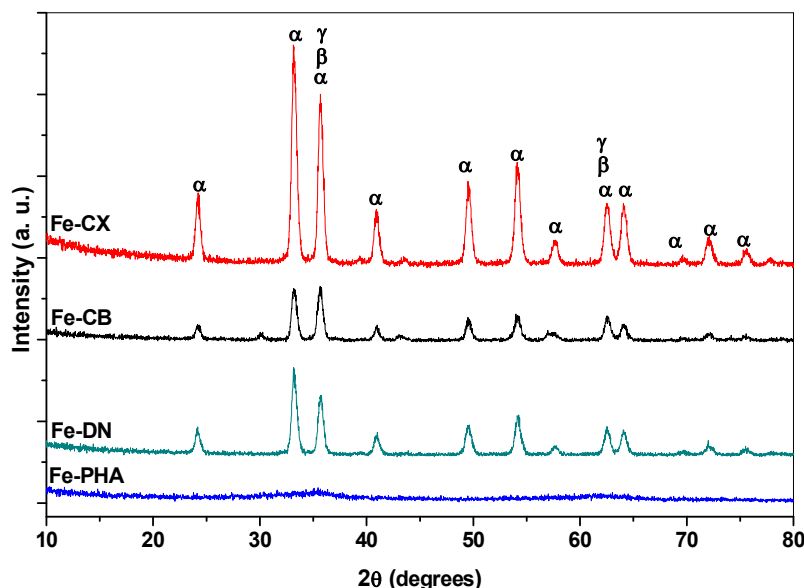
Figure 2 - XRD profiles of solids prepared by complexation (Fe-CX), combustion (Fe-CB), decomposition (Fe-DN), precipitation (Fe-PHA) and phases found:α = α-Fe₂O₃ (hematite), β = Fe₃O₄ (magnetite), γ = γ-Fe₂O₃ (maghemite).

Figure 3 - Color of samples obtained by precipitation (Fe-PHA), complexation (Fe-CX), combustion (Fe-CB) and decomposition (Fe-DN).

The solids presented isotherms IV (Figure 4), typical of mesoporous materials, whose main characteristic is hysteresis and the absence of nitrogen adsorption limitation at high $PP0^{-1}$ values. In addition, the samples presented hysteresis curves classified as H3, which is characterized by different evaporation and condensation paths between the adsorption and desorption processes undergone by the adsorbent materials. They showed levels for $PP0^{-1}$ values ranging from 0 to 0.8 and then a hysteresis branch in the region of high relative pressure with very steep slope, thus demonstrating multilayer formation and the presence of interparticle mesoporous, pores originated due to small crystals agglomeration. By analyzing the Fe-PHA sample pore size (Figure 4), a large, centered peak with 17 nm pore size distribution is observed. This mesopore can be attributed to interparticle pores due to crystals agglomeration. The other samples analyzed (Table 1) are also classified as

mesoporous (CAMPOS et al., 2015; HEITMANN et al., 2014).

Figure 5 shows the regions of the images obtained by SEM used for analysis by EDS. According to the spectra, the prepared solids indicated iron and oxygen elements presence in different samples analyzed. It can be observed that the determined values are different for the samples synthesized by different preparation methods with higher iron content for the sample obtained by the complexation method (Fe-CX). In addition, no contaminants were present in the samples analyzed (Figure 6). Different morphologies can be noted because of different synthesis methods. All samples were analyzed by scanning electron microscopy at 25 μm scale but the Fe-CX sample which was evaluated at 10 μm scale. In addition, according to SEM analysis it was observed that Fe-PHA and Fe-CX samples presented a rough surface with cracks and agglomerated particles on the surface. For Fe-CB and Fe-DN samples, a larger number of agglomerated particles was present

on the solids surface. These results corroborate the surface area and pore distribution analysis data, once the decrease in area values is related to samples pores partial coating.

3.1 Catalytic Activity

Figure 7 shows adsorption tests results, i.e., the decrease in methylene blue concentration in the absence of hydrogen peroxide. The maximum adsorption capacity was presented by the solid prepared by precipitation, followed by the solids prepared by complexation and decomposition. The solid prepared by combustion presented the lowest result. These results are consistent with the specific surface area values, that is, the adsorption capacity increased with the area.

Figure 8 shows the oxidation test curves, i.e., in the presence of peroxide versus time. In this case, the highest result was presented by the solid prepared by combustion. This was the solid whose system was most stable. Possibly, this result is associated with the presence of magnetite and maghemite phases for Fe-CB sample, as indicated by the magnetic bar test. This means that the combustion method led to a solid with a low area, disfavoring the adsorption process, however it produced Fe^{2+} species (PĂCURARIU et al., 2016), more active for the Fenton reaction.

Table 2 shows the removal, adsorption and oxidation values of the methylene blue dye after 180 min reaction. Thus, after this period, Fe-CB sample showed the highest result for oxidation. In general, all samples low catalytic activity can be attributed to the majority hematite phase that has been shown to be inactive compared to activation with hydrogen peroxide in order to produce more reactive species in organic compounds oxidation reactions under established experimental conditions. It has been reported in the literature that Fe^{2+} presence is extremely important for an active Fenton system (NOGUEIRA et al., 2007; SILVA et al., 2017) and hematite has solely Fe^{3+} in its structure. On the other hand, the sample obtained by the combustion method showed possible traces of magnetite, which partially compensated for its low specific surface area. The Fe-PHA sample adsorption values are consistent with the specific surface area values. Likewise, the sample prepared by combustion presents more magnetite phase than the others, thus it is more active for the oxidation test (ASHRAF et al., 2020).
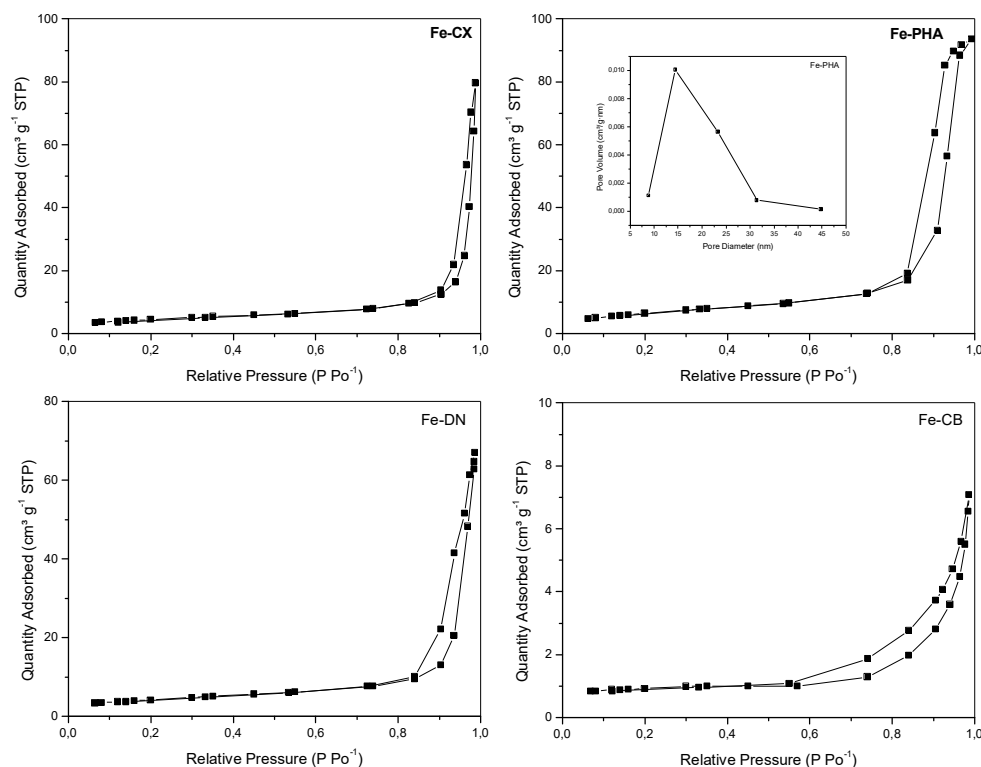
Figure 4 - N2 adsorption / desorption isotherms obtained by precipitation (Fe-PHA), complexation (Fe-CX), combustion (Fe-CB) and decomposition (Fe-DN).
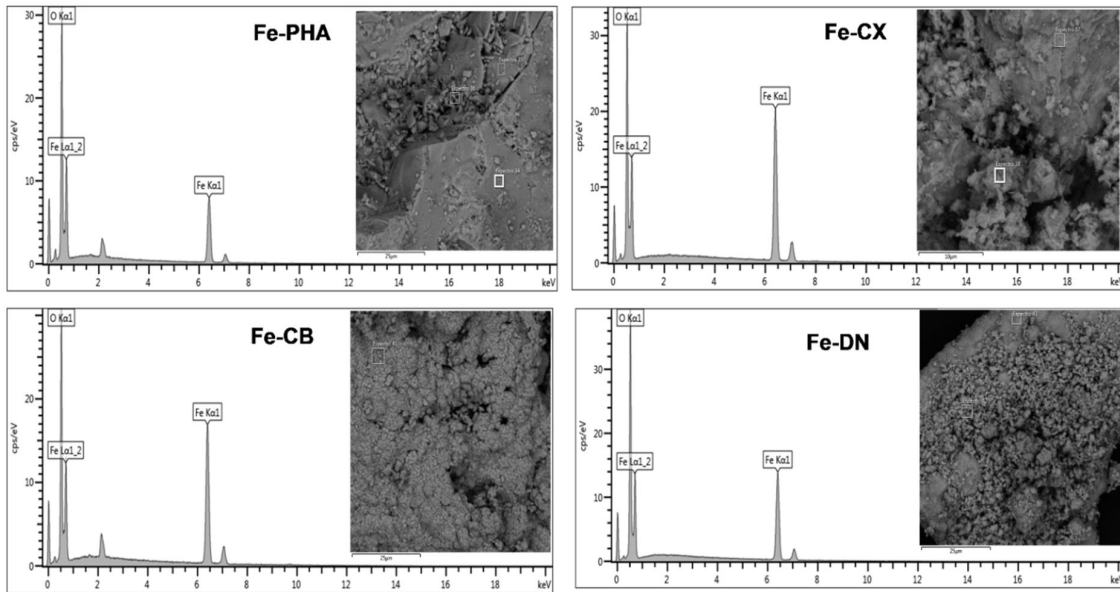
Figure 5 - EDS spectra and SEM images of solids obtained by precipitation (Fe-PHA), complexation (Fe-CX), combustion (Fe-CB) and decomposition (Fe-DN).
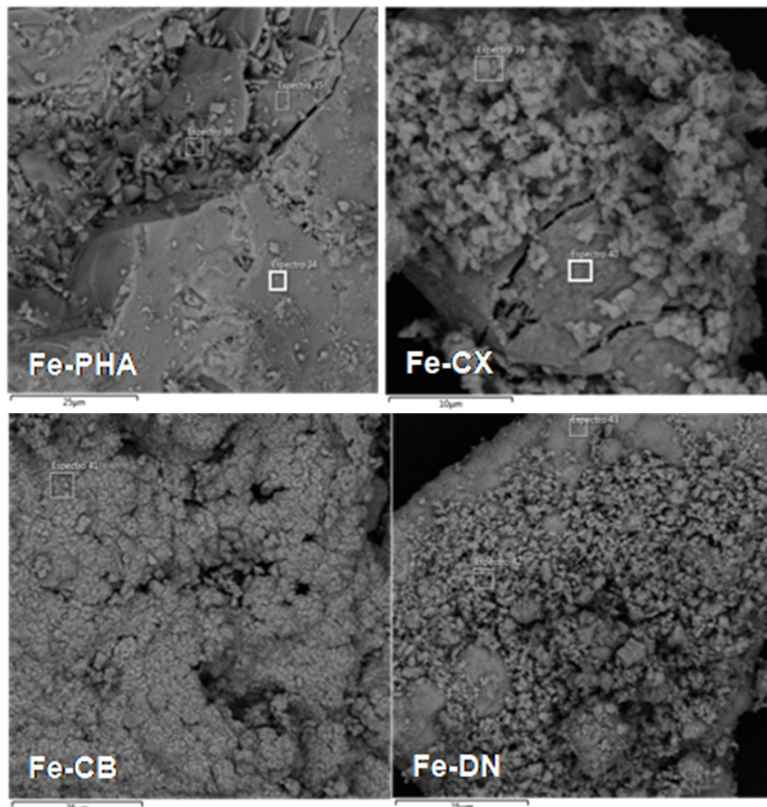
Figure 6 - SEM images of solids obtained by precipitation (Fe-PHA), complexation (Fe-CX), combustion (Fe-CB) and decomposition (Fe-DN); 3.00 kX of enlargement.
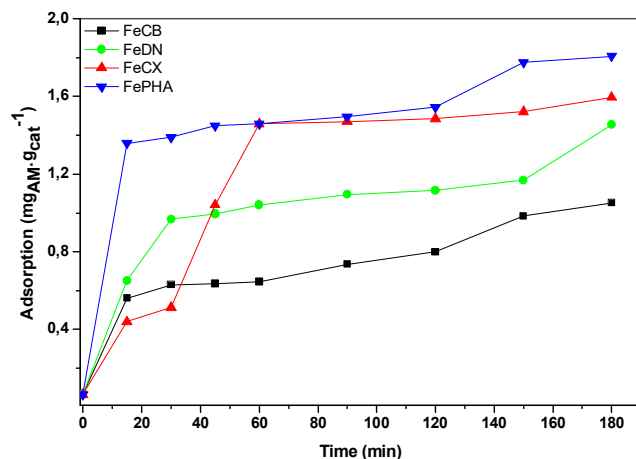
Figure 7. Adsorption of methylene blue on solids obtained by different methods: precipitation (Fe-PHA), complexation (Fe-CX), combustion (Fe-CB) and decomposition (Fe-DN).

Table 2 - Methylene blue adsorption and oxidation values after 180 minutes reaction.

Sample	Adsorption (%)	Oxidation (%)
Fe-PHA	18.07	19.80
Fe-CB	10.52	24.78
Fe-CX	15.96	17.41
Fe-DN	14.53	16.06
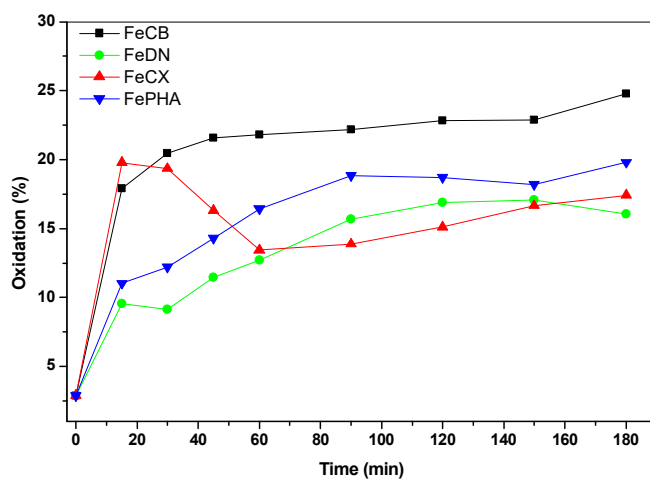
Figure 8 - Methylene blue dye oxidation by samples prepared through precipitation (Fe-PHA), complexation (Fe-CX), combustion (Fe-CB) and decomposition (Fe-DN).

4. CONCLUSIONS

Iron oxide catalysts were obtained by different methods (precipitation, complexation, combustion, and decomposition). It was observed that the catalytic properties of the solids were significantly influenced by the preparation method, being that:

(i) the preparation of solids by different methods favored hematite phase (α- Fe₂O₃) production with traces of magnetite (Fe₃O₄) and (γ- Fe₂O₃); (ii) the specific surface area varied according to the method and this effect was more effective for the sample obtained by ammonium hydroxide precipitation; (iii)

the solid prepared by precipitation showed the higher area and adsorption capacity, while the solid prepared by combustion showed more evidence of the presence of magnetite and higher activity in the oxidation reaction.

REFERENCES

ADANS, Y. F. et al. A simple way to produce gamma-Alumina from aluminum cans by precipitation reactions. Materials Research, v. 19, n. 5, p. 977–982, 2016.

ASHRAF, M. et al. Hematite and Magnetite Nanostructures for Green and Sustainable Energy Harnessing and Environmental Pollution Control: A Review. **Chemical Research in Toxicology**, v. 33, n. 6, p. 1292–1311, 2020.

ASSAF, M. et al. Catalytic evaluation of perovskite-type oxide LaNi1ÀxRuxO3 in methane dry reforming. **Catalysis Today**, v. 135, p. 129–135, 2008.

CAMPOS, E. A. et al. Synthesis, Characterization and Applications of Iron Oxide Nanoparticles - a Short Review. **Journal of Aerospace Technology and Management**, v. 7, n. 3, p. 267–276, 2015.

CARVALHO, L. S. et al. Preparation and characterization of Ru/MgO-Al2O3 catalysts for methane steam reforming. **Catalysis Today**, v. 142, n. 1–2, p. 52–60, 2009.

DENG, Y.; ZHAO, R. Advanced Oxidation Processes (AOPs) in Wastewater Treatment. Current Pollution Reports, v. 1, n. 3, p. 167–176, 2015.

DURIGAN, M. A. B.; VAZ, S. R.; PERALTA-ZAMORA, P. Degradation of emergent pollutants by Fenton and photo-Fenton processes. **Química Nova**, v. 35, n. 7, p. 1381–1387, 2012.

FERREIRA, H. S. et al. Redução catalítica seletiva de óxidos de nitrogênio sobre hematita contendo cobre. Química Nova, v. 30, n. 3, p. 611–615, 2007.

GARCÍA CERDA, L. A.; MONTEMAYOR, S. M. Synthesis of CoFe2O4 nanoparticles embedded in a silica matrix by the citrate precursor technique. **Journal of Magnetism and Magnetic Materials**, v. 294, n. 2, p. e43–e46, 2005.

GONÇALVES, M. et al. Synthesis and characterization of iron oxide nanoparticles supported on carbon matrix: oxidation of the dye methylene blue in water. **Química Nova**, v. 32, n. 7, p. 1723–1726, 2009.

HE, J. et al. Interfacial mechanisms of heterogeneous Fenton reactions catalyzed by iron-based materials: A review. **Journal of Environmental Sciences**, v. 39, p. 97–109, 2016.

HEITMANN, A. P. et al. Synthesis and characterization of a magnetic nanostructured composite containing manganese oxide for removal of Cd (II) from aqueous medium. **Cerâmica**, v. 60, n. 355, p. 429–435, 2014.

LIU, H. et al. Preparation and photo-fenton degradation activity of α-Fe2O3 nanorings obtained by adding H2PO4−, SO42−, and citric acid. **Chemical Engineering Journal**, v. 382, p. 123010, 2020.

MACHULEK, A. et al. Application of Different Advanced Oxidation Processes for the Degradation of Organic Pollutants. In: Organic Pollutants - Monitoring, Risk and Treatment. [s.l.] InTech, 2013.

MAGALHÃES, F. et al. Cr-containing magnetites Fe3-xCrxO4: The role of Cr3+ and Fe2+ on the stability and reactivity towards H2O2 reactions. **Applied Catalysis A: General**, v. 332, n. 1, p. 115–123, 2007.

MANENTI, D. R. et al. Otimização do processo foto-fenton utilizando irradiação artificial na degradação do efluente têxtil sintético. **Engevista**, v. 12, n. 1, 2010.

NOGUEIRA, R. F. P. et al. Fundamentos e aplicações ambientais dos processos fenton e foto-fenton. **Química Nova**, v. 30, n. 2, p. 400–408, 2007.

OLIVEIRA, L. C. A.; FABRIS, J. D.; PEREIRA, M. C. Iron oxides and their applications in catalytic processes: a review. **Química Nova**, v. 36, n. 1, p. 123–130, 2013.

PĂCURARIU, C. et al. Effective removal of methylene blue from aqueous solution using a new magnetic iron oxide nanosorbent prepared by combustion synthesis. **Clean Technologies and Environmental Policy**, v. 18, n. 3, p. 705–715, 23 2016.

PALÁCIO, S. M. et al. Combinação dos processos eletrocoagulação e fotocatálise heterogênea no tratamento de um efluente têxtil clorado. **Engevista**, v. 17, n. 3, p. 407, 2015.

PEREIRA, A. L. C. et al. Effect of iron on the properties of sulfated zirconia. **Applied Catalysis A: General**, v. 334, n. 1–2, p. 187–198, 2008.

SANTOS, D. P. B.; SILVA, C. T. Preparation, Characterization and Catalytic Evaluation of Niobium Oxide and Fe/Nb2O5 based-catalysts towards Blue Dye Oxidation by using Fenton reaction. **Exatas Online**, v. 6, p. 1–10, 2015.

SCHWERTMANN, H. C. U.; CORNELL, R. M. Iron Oxides in the Laboratary. Weinheim, Germany: Wiley-VCH Verlag GmbH, 2000.

SILVA, L. A. et al. Evaluation of nickel and copper catalysts in biogas reforming for hydrogen production in SOFC. **Matéria (Rio de Janeiro)**, v. 22, n. 1, p. 11802, 2017.

SILVA, M. K. et al. Evaluation of Nb2O5 and Ag/Nb2O5 in the photocatalytic degradation of dyes from textile industries. **Brazilian Journal of Chemical Engineering**, v. 19, n. 4, p. 359–363, 2002.

WANG, X. et al. Effect of glycine on one-step solution combustion synthesis of magnetite nanoparticles.

Journal of Alloys and Compounds, v. 719, p. 288–295, 2017.

ZANINI, F. A. et al. Aplicação do processo Fenton para descontaminação de hidrocarbonetos aromáticos em água. **The Journal of Engineering and Exact Sciences**, v. 3, n. 2, p. 184–196, 2017.

ZIMMERMANN, B. M. et al. Effect of thermal treatment on the catalytic activity of a Fe-rich bentonite for the photo-Fenton reaction. **Cerâmica**, v. 65, n. 373, p. 147–152, 2019.